

The influence of model surface roughness on wind loads of the RC chimney by comparing the full-scale measurements and wind tunnel simulations

Chern-Hwa Chen^{*1}, Cheng-Hsin Chang² and Yuh-Yi Lin²

¹Department of Civil and Environmental Engineering, National University of Kaohsiung, Kaohsiung, Taiwan
²Department of Civil Engineering, Tamkang University, New Taipei City, Taiwan

(Received August 11, 2009, Revised March 31, 2011, Accepted November 23, 2011)

Abstract. A wind tunnel test of a scaled-down model and field measurement were effective methods for elucidating the aerodynamic behavior of a chimney under a wind load. Therefore, the relationship between the results of the wind tunnel test and the field measurement had to be determined. Accordingly, the set-up and testing method in the wind tunnel had to be modified from the field measurement to simulate the real behavior of a chimney under the wind flow with a larger Reynolds number. It enabled the results of the wind tunnel tests to be correlated with the field measurement. The model surface roughness and different turbulence intensity flows were added to the test. The simulated results of the wind tunnel test agreed with the full-scale measurements in the mean surface pressure distribution behavior.

Keywords: chimney; full-scale measurement; Reynolds number; pressure; surface roughness; wind tunnel test

1. Introduction

The role of the Reynolds number was a crucial point in the development of the flows which study around rounded shapes. The flow fields varied with Reynolds number in the regions of the separation points, the nature of the wake, the vortex shedding, and wind pressures. Obviously, the drag coefficient of sharp edged shapes remained independent of the Reynolds number since the position of the separation points was fixed. The drag coefficient of the rounded object was influenced strongly by the flow conditions of higher Reynolds number, which were decreased in the region of the critical Reynolds number. This phenomenon defined the aerodynamic characteristics of rounded objects from lower Reynolds numbers to higher Reynolds numbers. Since the dimension of the objects and the wind velocity, the flow regimes of full-scale measurement were supercritical states and hypercritical states, whereas in wind tunnels, considering the simulation of the scaled-down model, flows were mostly subcritical and critical, not in accordance with full-scale measurement (Batham 1973).

Large wind-induced vibrations might occur in slender structures by effects of wind. Model tests were limited by their inability to use Reynolds numbers, preventing them from elucidating

*Corresponding author, Professor, E-mail: chchen@nuk.edu.tw

full-scale responses, since the effect of a high Reynolds number and turbulence at the vortex resonance could not be realized in the wind tunnel model. Therefore, full-scale measurements had to be made to confirm the real aerodynamic responses of structures under the effects of wind. Most studies of wind-induced vibrations of tall chimneys involved scaled-down models, rather than full-scale structures, which were tested in wind tunnels. The Reynolds number of field measurements of a chimney was of the order of 10^7 , which was in the supercritical region. In both wind tunnel experiments and full-scale field measurements, determining the flow around cylinders at such high Reynolds numbers was difficult. Therefore, very few comparison results was presented between full-scale field measurement and scaled-down model in wind tunnel test had, so the reliability of modeling approaches based on boundary layer wind tunnels thus remains uncertain.

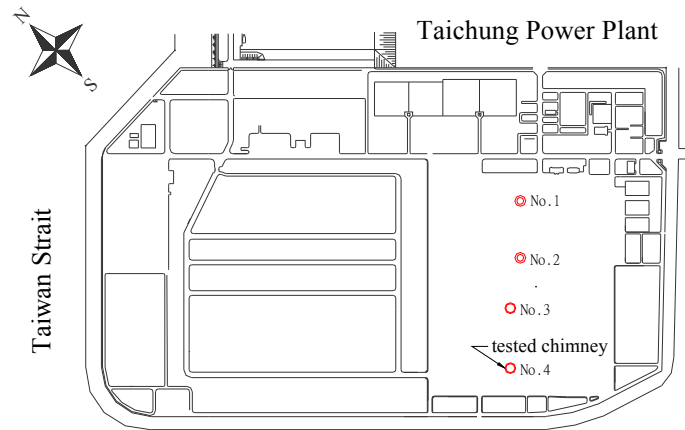
Kessler (1989) determined the wind forces and strains of RC chimney with a height of 230 m using full-scale measurements. Galemann and Ruscheweyh (1992), Ruscheweyh and Galemann (1996) measured wind-induced vibrations and wind pressures on a full-scale experimental steel chimney with a height of 28m and a diameter of 0.91m. Long-term full-scale measurements had also been made to determine cross-wind vibrations of four steel stacks in Germany (Ruscheweyh *et al.* 1998). Sanada *et al.* (1992) determined the characteristics of wind pressures and forces on a 200m chimney in the supercritical Reynolds number region from the full-scale measurements made during the effects of strong typhoon and monsoon winds. Many advanced works had adapted field measurement approaches to measure vortex-induced vibration (D'Asdia and Noe 1998) and the across-wind response (Waldeck 1992, Ciesielski *et al.* 1996) of a tall chimney. Much research had been performed into making full-scale measurements of chimneys, but questions remain concerning use of wind tunnel tests (Ciesielski and Oruba 1996). One of these questions concerned the effect of Reynolds number and vortex-induced vibration. The impossibility of simulating flows with high Reynolds numbers in boundary layer wind tunnels had prevented the study of flow around circular cylinders at high Reynolds numbers. Uematsu and Yamada (1995) investigated time-averaged wind loads on cantilevered circular cylinders at high Reynolds numbers in a wind tunnel test using rough-walled models. Van Koten and Pritchard (1986) determined crosswind motion of tall cylindrical structures using wind tunnel test. Fischer (1993) discussed wind induced vibrations of slender structures. Arunachalam *et al.* (2001) developed a new empirical method for correlating the values of root mean square lift coefficient and Strouhal number relevant to full-scale chimney conditions based on corresponding values on circular cylinders in properly simulated boundary layer wind tunnel results.

This work presented a wind tunnel model that involved an artificially surface roughness in different turbulent flows, to determine the characteristics associated with high Reynolds number in a wind tunnel test. This approach was adapted to simulate the supercritical flow in a wind tunnel test. The wind pressures on the chimney, determined from the wind tunnel tests, were compared with those determined by full-scale measurements. For simplicity, an isolated chimney would be considered. This work discussed the mean wind pressure distribution on an RC chimney.

2. RC chimney with height of 245 m

The experimental chimney was located at Taichung power station in the central of Taiwan. Fig. 1 showed the experimental chimney and the location of the site. As displayed in Fig. 2, the chimney was composed of an RC windshield and two steel flues. Table 1 presented the material

and geometric properties of the structure. The RC windshield was supported by the pile foundation, and each steel flue was supported by a steel frame below the breech opening, which in turn was supported by a common pile foundation. Seven-storey work platforms were constructed for the daily maintenance and inspection of the steel flues. Lateral restraining rods were installed at the heights of 79 m, 151 m and 235 m, to help to maintain the stability of the steel flues by enabling them to be tied to the RC windshield. Each of the rods had a diameter of 35 mm and was pinned at both ends to resist extension or shrinkage due to any change in temperature of the steel flues. The RC windshield was erected by the slip-forming construction. As presented in Fig. 3, the surface painted of the tested RC chimney is smooth.



(a)



(b)

Fig. 1 The experimental chimney and the situ of location: (a) plane view and (b) photo view



Fig. 3 Shape and surface of chimney

Table 1 Material and geometric properties of the prototype chimney

Item	Reinforced concrete windshield	Steel flue
Height	245 m	250 m
Material	Concrete $f_c=35\text{MPa}$ Main rebar $f_{sy}=420\text{MPa}$	A-36
Diameter	29.7 m at bottom and linearly decreased to 17.1 m at top	6.7 m
Thickness	600 mm at bottom and linearly decreased to 375 mm at level 80 m; 300 mm for the higher	10 mm for the level below 143.75 m; 8 mm for the higher

3. Full-scale measurements

To study the surface pressure distribution of the chimney under the wind, the full-scale measurements of wind pressures on the RC chimney, associated wind speeds were made for a flow with high Reynolds number in a wind tunnel test. This work considered the mean wind pressure distribution on the RC chimney. Accordingly, this section described mainly the field measurements of wind speeds and surface pressures on the RC chimney in a monsoon.

3.1. Experimental set-up

Fig. 2 displayed experimental devices of measuring of a chimney in the field. The X- and Y-directions presented the two horizontal directions. The vertical axis of the chimney was defined as a Z direction. Table 2 presented the sensors used to measure the wind speed data. Since the working platforms that were available for measurement were few, the sensors were placed at the level of the work platforms. The surface pressure distribution on the chimney was measured using the 24 pressure transducers installed at the elevations of 150 m (6F, $z/H=0.612$) and 180 m (8F,

$z/H=0.857$), where z was the elevation, and $H=245\text{m}$ was the height of the chimney. The wind speed data were obtained by using anemometers at heights of 150 m and 245 m, which were fixed on an RC wall of the windshield (Chen 2004). All measuring data were recorded simultaneously using a PC-based portable data acquisition system with 32 channels. The wind pressures, wind speeds and wind directions were recorded at two-hour intervals and a sampling rate of 20 Hz. The measuring data were recorded over 24 hours.

Many highly sensitive servo velocity sensors were employed to measure simultaneously the wind-induced vibration of the chimney. The resolution was of the order of 10^{-4} cm/s. The recording system was a PC-based portable data acquisition system with 16 channels, which could convert analogue signals to digital data. The sensors were placed on the every work platforms, displayed in Fig. 2. The 16 sensors were utilized simultaneously in testing. In the vibration test, the velocity of the chimney was be simultaneously measured in two horizontal directions (x - and y - directions), as presented in Fig. 2. The vibration data from each level were measured in each horizontal direction.

The response of the chimney was recorded at the same time as wind data were obtained at two-hour intervals and a sampling rate of 50 Hz. The response data and wind data were thus simultaneously recorded over 24 hours with 12 measurements (Chen *et al.* 2001). In this work, the mean wind pressure distribution discussed to simulate the effects of high Reynolds number flow in wind tunnel.

Table 2 Sensors for observation in wind condition

Item	Total quantity	Location
Propeller anemometer and wind vane	2	one at the top of chimney and the other at a height of 150 m ($z/H=0.612$)
Pressure transducer	24	twelve at a height of 150 m ($z/H=0.612$) and twelve at a height of 180 m ($z/H=0.735$), on the surface of chimney
Servo-velocity sensor	16	each two (x - and y - directions) at a level, eight levels (2F~9F)

3.2. Processing data to determine mean pressure distribution

The surface pressures on the RC chimney and the associated wind speeds and vibration responses in northeasterly monsoon winds were determined by full-scale measurement. Fig. 2 presented the azimuth angle of the pressure taps (θ) on the chimney. The pressure tap at azimuth angles of zero, namely station 1, was normal to the approaching flow, which was the north-easterly. Fig. 4 plotted a typical time histories of wind speed and wind direction obtained from the full-scale measurements, where U was the mean wind speed. Fig. 4(b) displayed the azimuth angle of the pressure taps (θ) on the surfaces of the cylinder, where the north-easterly wind direction is defined as zero degree. Fig. 4(a) indicated mean wind speed was stationary during testing. Fig. 4(b) reveals that the wind direction was stationary and northeasterly. Fig. 5 presented typical time histories of wind pressures obtained from full-scale measurements.

Fig. 6 plotted the distribution of the mean pressure coefficient, C_p , at a height of 210 m ($z/H=0.857$). The pressure coefficient was evaluated for 10 minutes at wind speeds of over 12 m/s.

The Reynolds number, (Re) ranges from 1.09 to 1.36×10^7 . As presented in Fig. 6, the angle of zero pressure was about 30° . The coefficient of peak suction was -1.75 at angle about $\theta=60^\circ$. The base pressure coefficient at the rear was -0.65 where $\theta \geq 120^\circ$. The values of the pressure coefficient thus obtained were between the two values observed in two advanced investigations (Galemann and Ruscheweyh 1992, Sanada *et al.* 1992).

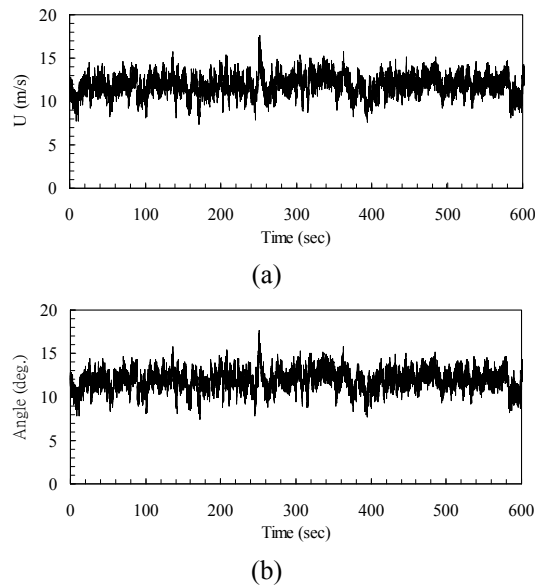


Fig. 4 A typical set of wind time history ($U=12.7\text{m/s}$): (a) wind speed and (b) wind direction

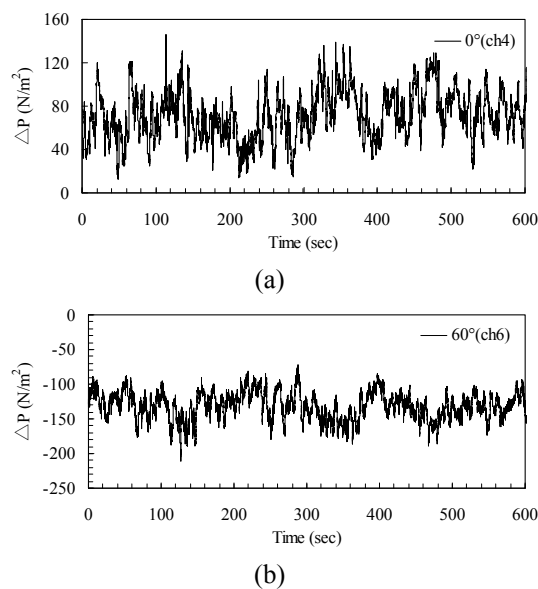


Fig. 5 A typical set of wind pressure ($U=12.7\text{m/s}$): (a) 0° and (b) 60°

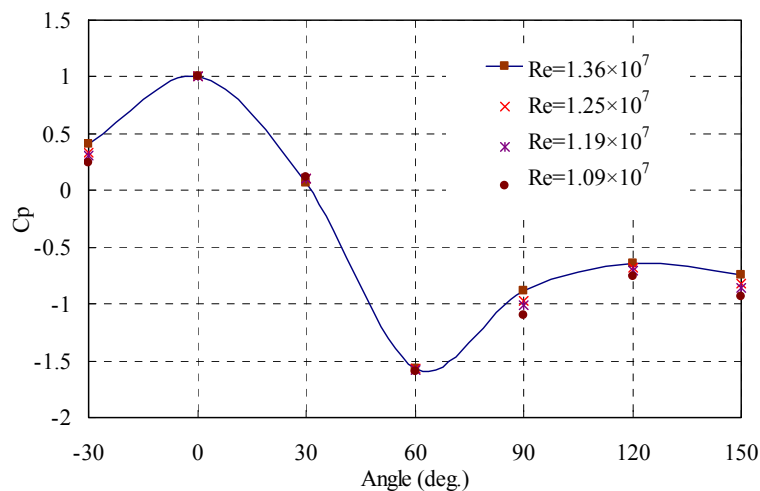


Fig. 6 Mean pressure distribution on full-scale measurement ($z/H=0.857$)

4. Wind tunnel experiments

To simulate the dynamic behavior of a chimney under wind flow with a large Reynolds number, the set-up and testing approach for the wind tunnel test were modified such that the results of the wind tunnel tests reflect closely the full-scale measurements. Both different surface roughness on the scaled-down model and turbulence intensity approaching flows would be used to suit the full-scale measurements of the surface pressure distribution in the wind tunnel test.

4.1. Wind tunnel setup

The experiments were performed at the atmospheric boundary layer wind tunnel laboratory of Tamkang University in Taiwan. The atmospheric boundary layer wind tunnel was an open-circuit, low-speed wind tunnel. The total length of the wind tunnel was 29.5 m; the test section was 18.7 m long, 3.2 m wide and 2.0 m high. A turntable (3.0 m in diameter) in the test section could be rotated easily to alter the direction of the approaching flow toward the model. A 175 hp, constant-speed motor, driving a 2.1m-diameter, variable-pitch fan generates a maximum wind speed of 18 m/s. The 4:1 contraction section contained honeycombs and four screens to generate low-turbulence flow at the entrance of the test section. Further, limited equipments was available for simulating of suitable boundary layer flow, two approaching boundary layers flow were used; one was a turbulent boundary layer with a turbulence intensity $I_u=3.9\%$ and $\alpha=0.18$, and the other one was a turbulent boundary layer with a turbulence intensity $I_u=4.8\%$ and $\alpha=0.15$, where α was the power law exponent dependent upon roughness of terrain. Two approach flows of the boundary layers were suitable for open terrain with monsoon.

4.2. Model configurations

Table 3 presented the geometrical and scaled-down properties of the model. 1:190 scaled-down models were adapted to determine the distribution of surface pressure in the wind tunnel test. Four artificially surfaces roughness were employed to simulate artificial flow field features past a cylinder, representing the characteristics of flows with high Reynolds numbers. Table 4 presented the material and geometric properties of four artificially surfaces roughness. Fig. 7 showed the photos of four artificially surfaces roughness. Based on the equivalent sand roughness, Achenbach (1970) defined the standard roughness to elucidate the effects of the aspect ratio and the surface roughness on the circumferential pressure distribution. In the present work, the aspect ratio H/D of the chimney was varied from 8.25 (at 9F level) to 14.33 (at 1F level), where H was the height of the chimney, and D was the diameter of the chimney, which varies with the elevation. Based on the equivalent sand roughness, the roughness of a uniform surface could be defined as follows

$$Sr = k_s / D \quad (1)$$

where k_s was the equivalent coefficient of sand roughness. However, the equivalent sand roughness could not be used to define a discrete artificially roughened surface. In this work, a laser displacement sensor could be adopted directly to measure the roughness of surfaces. The general equivalent roughness of a surface was defined as follows; (Chen 2005)

$$\bar{k}_s = \sum s / \bar{L} \quad (2)$$

Table 3 Properties of scaled-down model in wind tunnel (1:190)

Height z		Diameter D		Prototype Level	z/H	Model No. of pressure hole
Prototype (m)	Model (cm)	Prototype (m)	Model (cm)			
245	128.95	17.10	9.00	9F	1	/
230	121.05	17.87	9.41	/	0.958	24
210	110.53	18.90	9.95	8F	0.857	36
180	94.74	20.44	10.76	7F	0.735	24
150	78.95	21.99	11.57	6F	0.612	36
120	63.16	23.53	12.38	5F	0.490	/
0	0	29.70	15.63	1F	0	/

Table 4 Properties of four artificially roughness surfaces for scaled-down model (z/H=0.857)

Category	Type	Attachment		Surface roughness (Sr)
		Material		
k_1	Uniform	Sandpaper (No. 40)		$7.635 \cdot 10^{-3}$
k_2	Uniform	Small-bore gravel		$8.646 \cdot 10^{-3}$
k_3	Discrete	PVC tube at intervals 10 deg ($\psi=2.4\text{mm}$)		$1.022 \cdot 10^{-2}$
k_4	Discrete	PVC tube at intervals 10 deg ($\psi=3.3\text{mm}$)		$1.390 \cdot 10^{-2}$

where \bar{L} was the measured length of the artificially roughened surface, and Σs was the sum of scanned heights of the roughness in the measured region. Therefore, Eq. (1) could be adopted directly to describe a discrete artificially roughened surface through using Eq. (2). As presented in Table 4, the four relative surfaces roughness were evaluated similarly. The roughness of the uniformly roughened surface was of the order of 10^{-3} . That of the discretely roughened surface was of the order of 10^{-2} . Therefore, the discretely surfaces roughness had a higher roughness than the uniformly surfaces roughness.

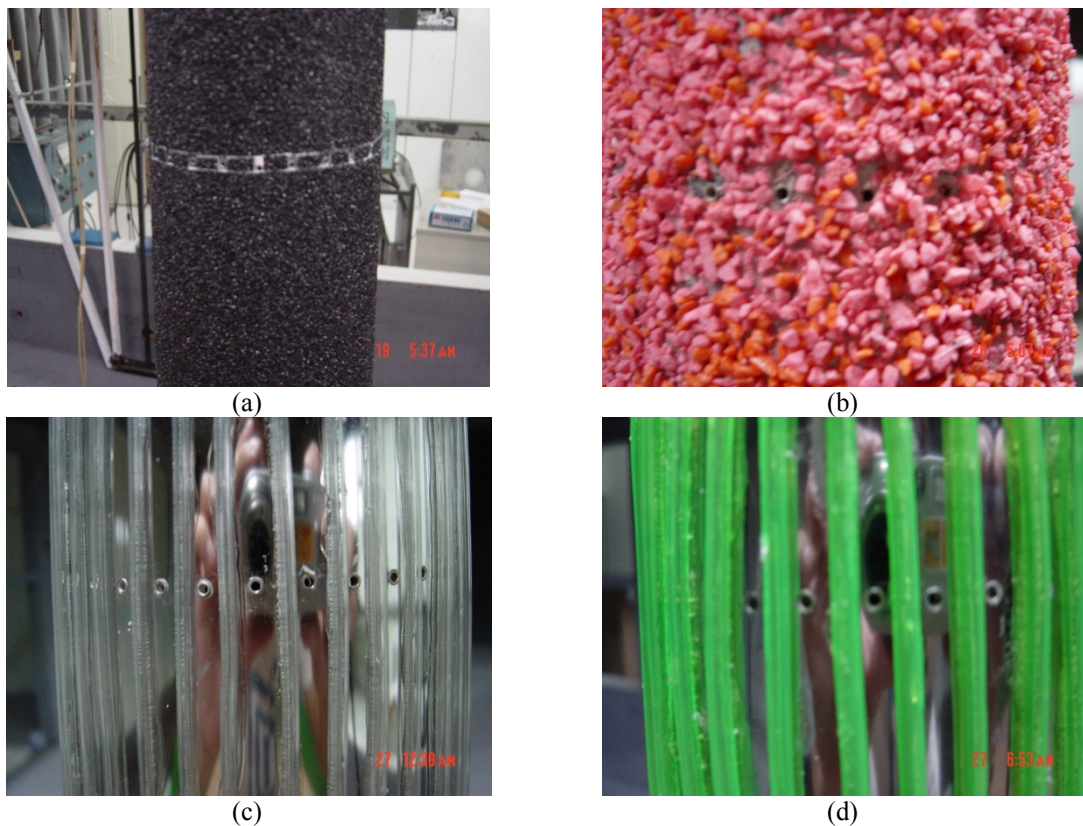


Fig. 7 The photos of four artificially roughened surfaces: (a) No. 40 Sandpaper (k_1 type), (b) Small-bore gravel (k_2 type), (c) PVC tube at intervals 10 deg ($\psi=2.4\text{mm}$) (k_3 type) and (d) PVC tube at intervals 10 deg ($\psi=3.3\text{mm}$) (k_4 type)

4.3. Results of case with high Reynolds number

In this study, the different surface roughness of the model was adopted to simulate artificially boundary layer flows with high Reynolds numbers in the wind tunnel test. Since limited equipments was available for simulating boundary layer flow in the wind tunnel test, two turbulence intensity approaching flows were employed, a turbulent boundary layer with turbulent

intensity $I_u=3.9\%$ and $\alpha=0.18$, and a turbulent boundary layer with turbulent intensity $I_u=4.8\%$ and $\alpha=0.15$.

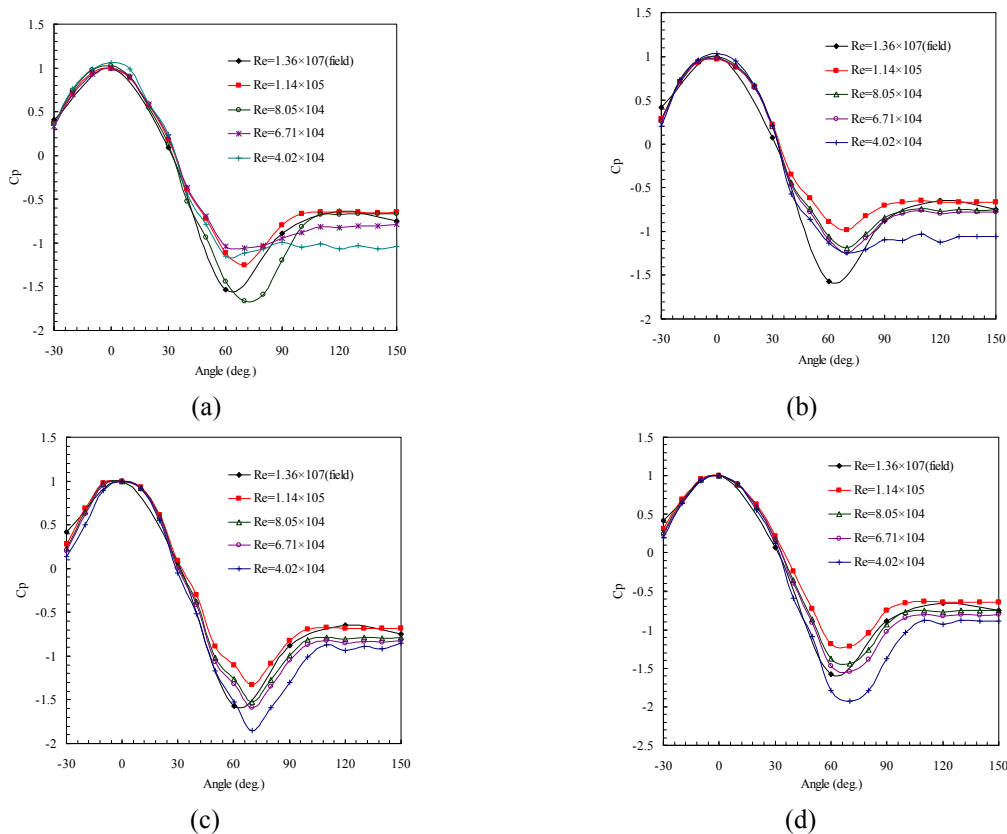


Fig. 8 Comparison of wind pressures with full-scale measurement in wind tunnel test ($I_u=3.9\%$, $\alpha=0.18$, $z/H=0.857$): (a) roughened surface k_1 , (b) roughened surface k_2 , (c) roughened surface k_3 and (d) roughened surface k_4

Fig. 8 showed the mean pressure coefficients at $z/H=0.857$, determined for four surfaces roughness under turbulent flows with turbulent intensity $I_u=3.9\%$ and $\alpha=0.18$. Figure 8 indicated that most of these experiments were performed at Reynolds numbers between the high 10^4 s and the low 10^5 s in the wind tunnel test. The Reynolds numbers in fact ranged from 4.02×10^4 to 1.14×10^5 . The roughness k_1 was that of the uniform surface obtained using a sandpaper material. The roughness k_2 is that of uniform surface obtained using small-bore gravel. Figs. 8(a) and (b) reveal that the angular position of zero pressure crossing was 30~40 degrees agreeing with the angular range obtained in the field measurements. The coefficient of peak suction varied with Re. The base pressure coefficient did not match those obtained in the field measurements. Accordingly, the results of the pressure distribution obtained using the two types of uniform

surface roughness were not highly consistent with the simulated of characteristics of flows with subcritical Reynolds numbers in the wind tunnel.

Figs. 8(c) and (d) plotted the simulation results obtained using the two discrete artificially surfaces roughness. The roughness k_3 was that of the discrete surface obtained using a PVC tube with a diameter of 2.4 mm at intervals 10 degrees to paste down around the surface of circular model. Roughness k_4 was that of a discrete surface roughness obtained using PVC tube with a diameter of 3.3mm at intervals 10 degrees to paste down around the surface of circular model. Fig. 8(c) indicated that the pressure distribution associated with roughness k_3 at Reynolds numbers between $6.71 \times 10^4 \sim 1.14 \times 10^5$ was similar to that associated with flows at supercritical Reynolds numbers, as typically determined by the full-scale measurements, but the angular position of the peak suction did not match closely. Fig. 8(d) indicated the pressure distribution associated with roughness k_4 at Reynolds numbers in the region $6.71 \times 10^4 \sim 1.14 \times 10^5$ was similar to that associated with supercritical Reynolds number flows, as generally determine by the full-scale measurements. Therefore, the highest roughness of the surface (k_4) could be adopted to simulate flow with supercritical Reynolds numbers in a wind tunnel test with lower Reynolds numbers.

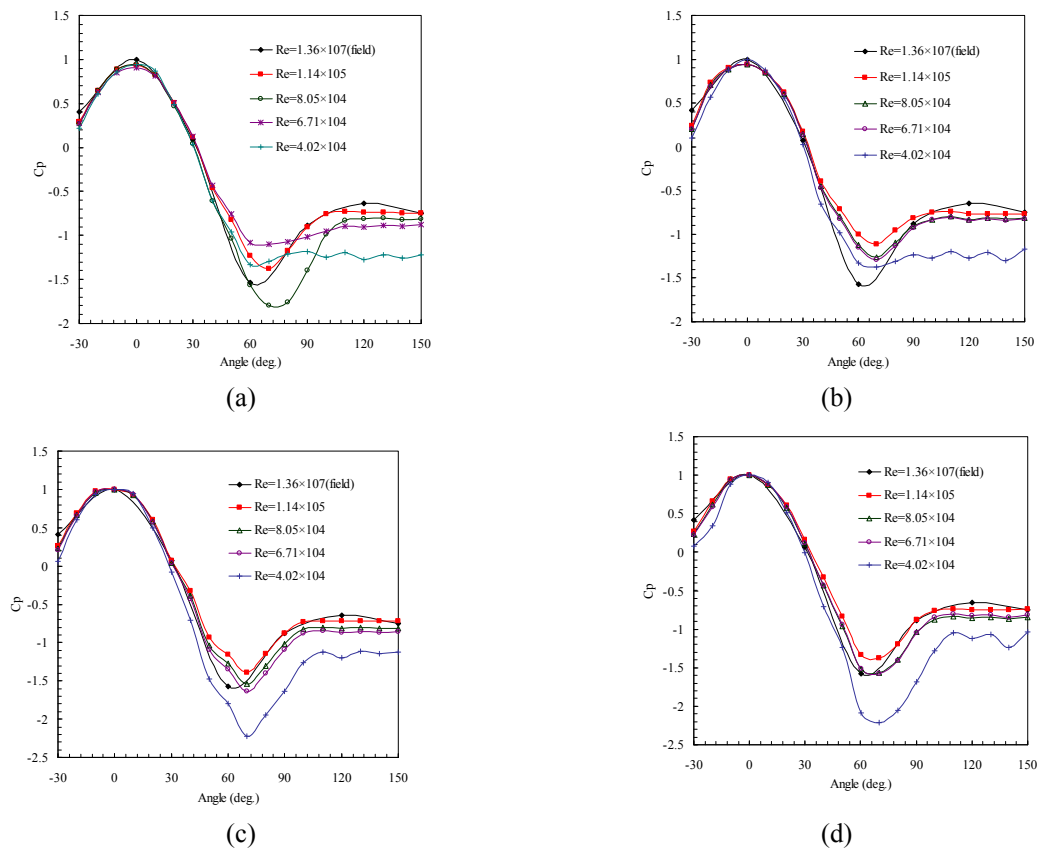


Fig. 9 Comparison of wind pressures with full-scale measurement in wind tunnel test ($I_u=4.8\%$, $\alpha=0.15$, $z/H=0.857$): (a) roughened surface k_1 , (b) roughened surface k_2 , (c) roughened surface k_3 and (d) roughened surface k_4

To investigate the effect of turbulent intensity for simulation of characteristics of flows in wind tunnel test, a turbulent boundary layer with a turbulent intensity $I_u=4.8\%$ ($\alpha=0.15$) was adopted to determine the mean wind pressure coefficient for the four different surfaces roughness, as presented in Fig. 9. A comparison with two turbulent intensity cases revealed that the result simulated in the wind tunnel test exhibited an improvement in the coefficient of peak suction by at high turbulent intensity. From Fig. 9(d), the roughness k_4 yielded an excellent wind pressure distribution agreeing with the angular range obtained in the field measurements. The pressure distribution obtained using roughness k_3 represents Reynolds numbers between $6.71 \times 10^4 \sim 1.01 \times 10^5$ that associated with flow of the field-scale measurements of pressure distribution. Accordingly, the roughness k_4 was very similar to the full-scale measurements of pressure distribution, as presented in Fig. 9(c). Therefore, a minimum Reynolds number of 6.71×10^4 was required to produce the above flow features. Moreover, Fig. 10 showed that with $Re=1.14 \times 10^5$ and $I_u=4.8\%$, the better accuracy guaranteed including the location of the angle of zero pressure, the coefficient of peak suction and the base pressure while compared with the field measurement ($Re=1.36 \times 10^7$ field).

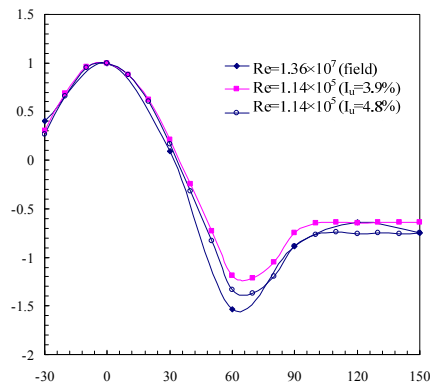


Fig. 10 Comparison of wind pressures with full-scale measurement in the different turbulence intensities of wind tunnel test by using roughened surface k_4

5. Effects of surface roughness

Figs. 8 and 9 plotted the mean pressure coefficients (C_p) around the cylinders obtained from wind tunnel tests. The results obtained using the cylinders with k_4 roughness are the closest to the field measurements. To study the effects of surface roughness on the similarity between aerodynamic test models, the characteristics of the surface pressure on the cylinder models had to be examined further. There were no fluctuation data from the field measurements. Hence, the study only presented the comparisons between the smooth surface and the surface roughness k_4 of the chimney for fluctuation data, such as C_p' and PDF.

5.1. Fluctuating pressure coefficients

Figs. 8 and 9 showed the surface pressures with azimuth angles of over 30 degree, the surface pressure changes to the negative values that cause separating flow shedding behaviors (Cheng and Kareem 1992). Fig. 11 plotted the fluctuating pressure coefficients (C_p') around the cylinders. The figure indicated that the surface roughness of the cylinder did not significantly affect the distribution of the fluctuating pressure coefficients. However, the distribution of (C_p') on the cylinder with a smooth surface seemed to be scattered. The large fluctuating pressure coefficients arose from the unstable vortex shedding effect on the sides.

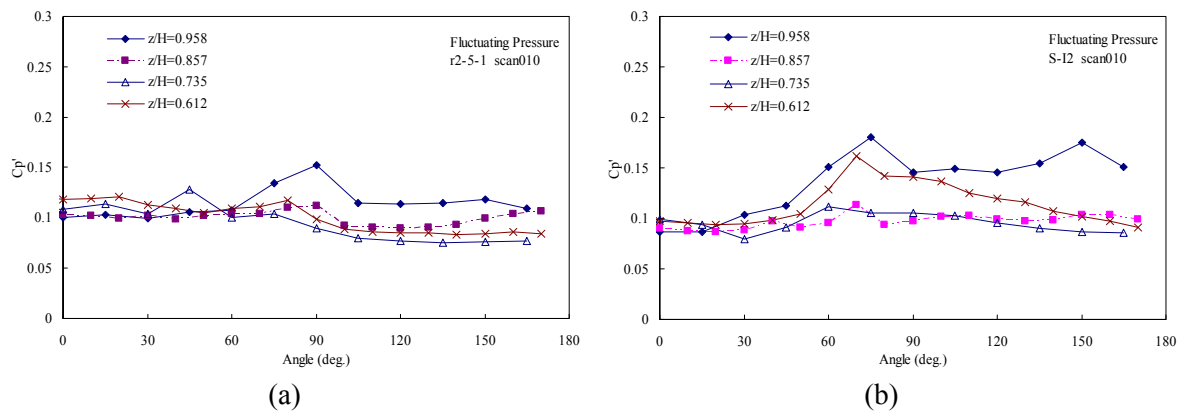


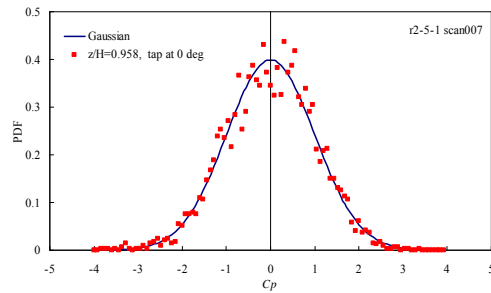
Fig. 11 The distribution of fluctuating pressure coefficients around the cylinders ($I_u=4.8\%$, $\alpha=0.15$, $Re=1.14\times 10^5$): (a) cylinder surface with k_4 roughness and (b) cylinder with smooth surface

5.2. Probability density functions

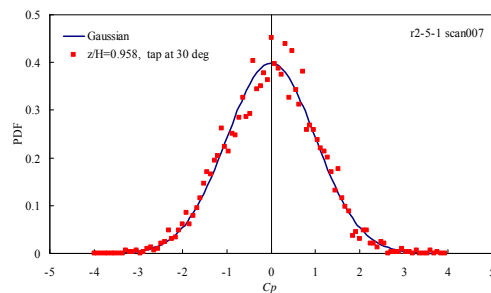
Figs. 12 and 13 plotted the probability density function (PDF) of wind pressure for some pressure taps. As the figures showed, the PDFs of pressures on the front and side of the cylinder were very close to Gaussian distribution. The PDF of pressure measured at various heights, presented in Fig. 13, was also quite close to Gaussian distribution. These figures showed that the PDFs of fluctuating pressures with height and circular area did not differ substantially.

5.3. Power spectrum and spatial correlation of surface pressures

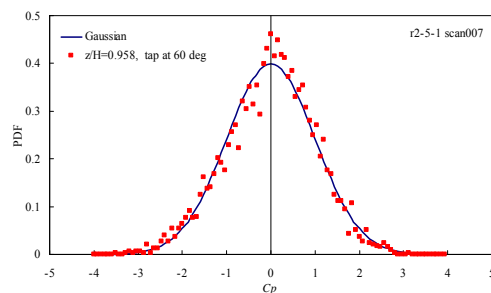
Fig. 14 plotted the power spectrum density function of surface pressures at various azimuth angles, where f is the frequency. The spectrum was of the broad-band type. The peak vortex shedding in each pressure spectrum at azimuth angles of 0 degree, 60 degree and 180 degree with a turbulent intensity of 4.8% was not intense. The vortex shedding of the separation shear layer was heavily disturbed by the turbulent fluctuations of the approaching flow.



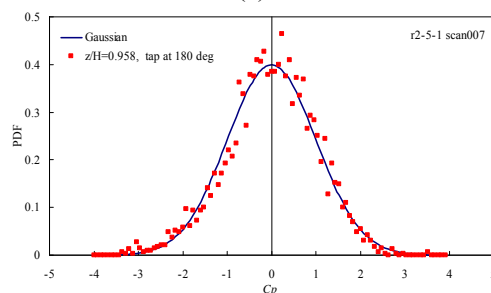
(a)



(b)



(c)



(d)

Fig. 12 The PDF of fluctuating surface pressures at $z/H=0.958$ height of the cylinder with k_4 surface roughness ($I_u=4.8\%$, $\alpha=0.15$, $Re=1.14\times 10^5$). The azimuth angle θ is: (a) 0 degree, (b) 30 degree, (c) 60 degree and (d) 180 degree

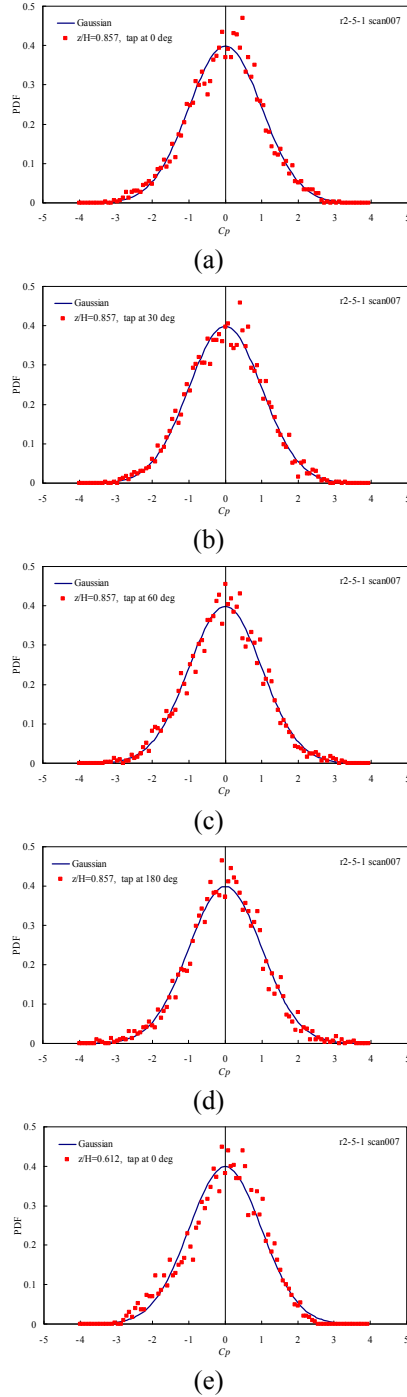


Fig. 13 The PDF of fluctuating surface pressures at variant heights of the cylinder with k_4 surface roughness ($I_u=4.8\%$, $\alpha=0.15$, $Re=1.14\times 10^5$): (a) the azimuth angle is 0 degree and $z/H=0.875$, (b) the azimuth angle is 30 degree and $z/H=0.875$, (c) the azimuth angle is 60 degree and $z/H=0.875$; (d) the azimuth angle is 180 degree and $z/H=0.875$; (e). the azimuth angle is 0 degree and $z/H=0.612$

The coefficient of spatial correlation along the circle around the cylinder was defined as

$$R_{ij} = \sum_{j=1}^N \left[\frac{(p_i - \bar{p}_i)(p_j - \bar{p}_j)}{\sigma_{p_i} \sigma_{p_j}} \right] / N \quad (3)$$

where R_{ij} was the coefficient in the spatial correlation of pressure; p was the surface pressures; \bar{p} was the mean surface pressure; σ_p was the coefficient of variation, and N was the total number of samples.

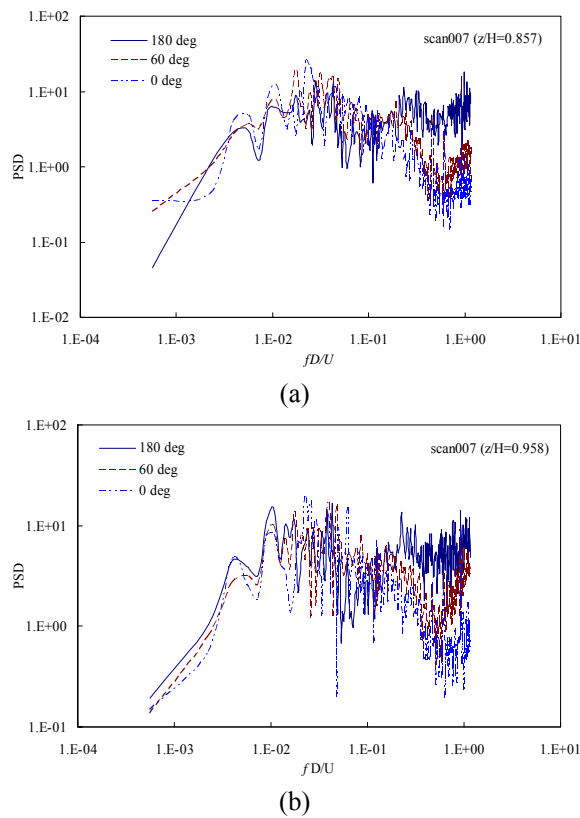
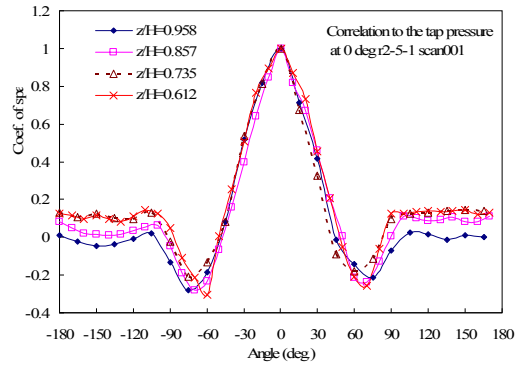


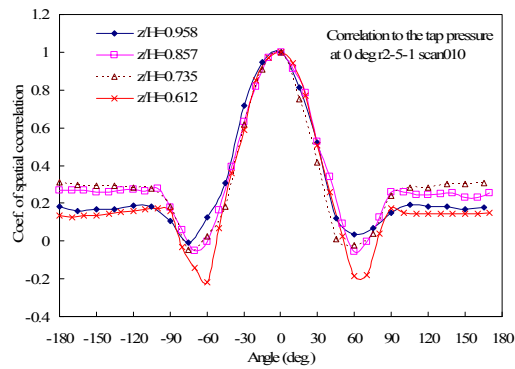
Fig. 14 The power spectral density function of fluctuating surface pressures at variant heights of the cylinder with k_4 surface roughness ($Re=8.5 \times 10^4$): (a) $z/H=0.875$ and (b) $z/H=1$

The coefficient of spatial correlation of pressure (R_{ij}) at the tap from at an azimuth angle of zero to at the other location was discussed. Fig.15 plotted the coefficient of spatial correlations of surface pressure at same height. The Re values in Figs. 15(a) and (b) were 4.02×10^4 and 1.14×10^5 , respectively, and the surface roughness was k_4 in each cases. Figure 15 indicated that the R_{ij} values of surface pressure at various heights were quite similar. The Re values in Fig. 15(c) was 1.14×10^5 , and the surface of the cylinder was smooth. Fig. 15(c) indicated that the R_{ij} values of surface

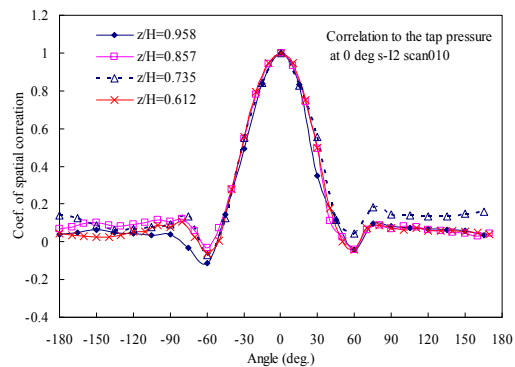
pressure at azimuth angles of under ± 30 degrees were similar to those of the roughened surfaces. However, the R_{ij} values of the surface pressures at azimuth angles of greater ± 30 degrees were close to zero. The simulation of the shear layer that was generated on a smooth surface of a cylinder departs from that of a roughened cylinder. The behavior of the separation shear layer in the side and back zones of the cylinder could not be characterized accurately.



(a)



(b)



(c)

Fig. 15 The coefficients of correlation of zero azimuth pressure tap to the different zone: (a) the surface roughness is k_4 and $Re.$ is 4.02×10^4 ; (b) the surface roughness is k_4 and $Re.$ is 1.14×10^5 ; (c) the surface of cylinder is smooth $Re.$ is 1.14×10^5

As discussed above, pasting a PVC tube on the surface of a cylinder, which increases the surface roughness, could improve the effect of simulation for high Reynolds numbers. The results of aerodynamic test effectively reflected the behavior of supercritical flow in field measurements. The best wind tunnel model in the study was with the surface roughness k_4 and the approaching wind profile with $I_u=4.8\%$. Due to the fluctuation of the surface pressure was not collected and the limitation of the pressure collecting system. The study could not provide the comparisons of the fluctuation pressures between the field measurement and the wind tunnel tests. However, the study presented the comparisons between the smooth surface and the surface roughness k_4 of the chimney for fluctuation data, such as C_p' and PDF (see Figs. 11-15). The work provided an approach that the mean surface pressure distribution behavior of chimney under natural flow with a larger Reynolds number could be approximated in the wind tunnel test by changing the surface roughness of the chimney.

6. Conclusions

In this work, the full-scale measurements of wind speeds, directions, and pressure for existing chimneys were made. Then, the wind characteristics in the field and the circumferential mean wind pressure around the chimney could be determined. The next step, the different surface roughness of the scaled-down model could be adopted effectively to simulate flows with high Reynolds numbers in a wind tunnel test. The highest value of the discretely surface roughness could be adopted to simulate flow with supercritical Reynolds numbers in a wind tunnel test with lower Reynolds numbers. Accordingly, the wind characteristics in the field and the circumferential mean surface pressure on the chimney could be reconstructed in a wind tunnel test. The results of the wind tunnel test effectively reflected the behavior of supercritical flow in the field measurements. In the future, the approaches developed herein would be further applied to an aeroelastic scaled-down model of a chimney to study the dynamic behavior of tall chimneys under wind loads.

Acknowledgements

The authors would like to thank the National Science Council of the Republic of China for financially supporting this research under Contract No. NSC91-2211-E-033-007, No. NSC92-2211-E-390-009, and NSC93-2211-E-390-008.

References

- Achenbach, E. (1970), "Influence of surface roughness on the cross-flow around a circular cylinder", *J. Wind Eng. Ind. Aerod.*, **64**(2), 321-335.
- Arunachalam, S., Govindaraju, S.P., Lakshmanan, N. and Appa Rao, T.V.S.R. (2001), "Across-wind aerodynamic parameters of tall chimneys with circular", *Eng. Struct.*, **23**, 502-520.
- Batham, J.P. (1973), "Pressure distributions on circular cylinders at critical Reynolds number", *J. Fluid Mech.*, **57**(2), 209-228.
- Chen, C.H., Huang, C.S. and Huang, C.T. (2001), "Modal identification of chimney using subspace approach", *J. Struct. Eng.*, Taipei, Taiwan, **16**(4), 99-117. (in Chinese)

- Chen, C.H. (2004), "Seismic assessment of a retrofitted chimney by FEM analysis and field testing", *Int. J. Struct. Stability Dynam.*, **4**(3), 337-359.
- Chen, C.H. (2005), "Simulation of high Reynolds number of wind tunnel test of RC chimney", *Proceedings of the 6th Asia-Pacific Conference on Wind Engineering, APCWE6*, September 2-4, Seoul, Korea.
- Cheng, C.M. and Kareem, A. (1992), "Across wind response of reinforced concrete chimneys", *J. Wind Eng. Ind. Aerod.*, **41-44**, 2141-2152.
- Ciesielski, R., Flaga, A. and Kawecki, J. (1996), "Aerodynamic effects on a non-typical steel chimney 120 m high", *J. Wind Eng. Ind. Aerod.*, **65**(1-3), 77-86.
- Ciesielski, R. and Oruba, R. (1996), "Low-speed wind gusts used for experimental evaluation of eigenfrequencies of tall reinforced concrete chimneys", *J. Wind Eng. Ind. Aerod.*, **65**(1-3), 97-106.
- D'Asdia, P. and Noe, S. (1998), "Vortex induced vibration of reinforced concrete chimneys: in situ experimentation and numerical provisions", *J. Wind Eng. Ind. Aerod.*, **74-76**, 765-776.
- Fischer, O. (1993), "Some comments to wind induced vibrations of slender structures", *J. Wind Eng. Ind. Aerod.*, **48**(2-3), 135-143.
- Galemann, T. and Ruscheweyh, H. (1992), "Measurements of wind induced vibrations of a full-scale steel chimney", *J. Wind Eng. Ind. Aerod.*, **41-44**, 241-252.
- Kaweckia, J. and Żurański, J.A. (2007), "Cross-wind vibrations of steel chimneys - A new case history", *J. Wind Eng. and Ind. Aerod.*, **95**(9-11), 1166-1175.
- Kessler, H. (1989), "Wind forces and strains of reinforced concrete chimneys", *J. Wind Eng. Ind. Aerod.*, **32**, 181-187.
- Ruscheweyh, H. and Galemann, T. (1996), "Full-scale measurements of wind-induced oscillations of chimneys", *J. Wind Eng. Ind. Aerod.*, **65**(1-3), 55-62.
- Ruscheweyh, H., Langer, W. and Verwiebe, C. (1998), "Long-term full-scale measurements of wind-induced vibrations of steel stacks", *J. Wind Eng. Ind. Aerod.*, **74-76**, 777-783.
- Sanada, S., Suzuki, M. and Matsumoto, H. (1992), "Full-scale measurements of wind force acting on a 200m concrete chimney, and chimney response", *J. Wind Eng. Ind. Aerod.*, **41-44**, 2165-2176.
- Uematsu Y. and Yamada M. (1995), "Effect of aspect ratio and surface roughness on the time-averaged aerodynamic forces on cantilevered circular cylinders at high Reynolds number", *J. Wind Eng. Ind. Aerod.*, **54-55**, 301-312.
- Van Koten, H. and Pritchard, B.N. (1986) "Predicting crosswind movements of chimneys", *J. Wind Eng. Ind. Aerod.*, **23**, 477-485.
- Waldeck, J.L. (1992), "The measured and predicted response of a 300 m concrete chimney", *J. Wind Eng. Ind. Aerod.*, **41-44**, 229-240.